Dual-channel ratiometric colorimetric sensor array for quantification and discrimination of o-, m- and p-phenols

Chengwu Lan
Jilin University of Chemical Technology
Lei Meng
Jilin University of Chemical Technology
Na Xu (xn_1216@163.com)
Jilin University of Chemical Technology

Research Article

Keywords: sensor array, ratiometric, colorimetric, phenols, peroxidase, Cu2(OH)3Cl

Posted Date: May 9th, 2022

DOI: https://doi.org/10.21203/rs.3.rs-1611519/v1

Abstract

The determination of trace o-, m- and p-phenols in food samples was of great significance, but it is still very challenging due to the low concertation and complex matrix. In comparison to traditional sensors based on “Lock-and-key” strategy, the sensor arrays that mimicked human olfactory system exhibited excellent universality and efficiency in assays of structural analogues. Herein, we described a costless and robust colorimetric sensor array for ratiometric quantification and discrimination of o-, m- and p-phenols. The obtained $Cu_2(OH)_3Cl$ with peroxidase-like (POD) activity was served as nanozyme to accelerate oxidation of 3,3’,5,5’ -tetramethylbenzidine (TMB) with H_2O_2. UV-vis absorbance spectroscopy displayed remarkable enhancements both at 652 nm and 450 nm, individually attributable to formation of single and dual electron-oxidized TMB (TMBox) substances. Then varied phenols regulated the absorbance *via* specific electron transfer processes. With the two peaks as dual signals, a ratiometric colorimetric sensor was designed to monitor different phenols. The ratio (I_{652}/I_{450}) was recorded to quantify phenols sensitively, where internal reference ruled out interferences from environment and equipment. Moreover, a ratiometric colorimetric sensor array was also explored for simultaneous discrimination of o-, m- and p-phenols. By integrating with colorimetric fingerprints and principal component analysis (PCA), each phenol was distinctly discriminated even at a very low concentration. This work demonstrated the reliability of a ratiometric colorimetric sensor array for identification of multiple phenols.

1. Introduction

As the basic raw materials and intermediates of organic chemistry industry, phenols were wildly applied in the petrochemical industry, food processing, and medicine. Nevertheless, discharge of these pollutants to the environment received increasing attention due to the extreme toxicity and low biodegradability (Arfin et al. 2019). Those residual phenols in food contact materials might easily migrate to food due to that they were in the form of physical combination with polymer rather than a covalent bond (Du et al. 2016). Considering the negative effects on nervous urinary, and digestive systems in humans (Michałowicz and Duda 2007), it’s urgent to develop a simple, accurate, and cost-effective method to quantify and discriminate series of phenols.

Until now, a series of analytical techniques as chromatography (Chernonosov et al. 2017), fluorescence spectroscopy (Qi et al. 2018), immunoassay (Karim and Fakhruddin 2012) and electrochemical analysis (Cheng et al. 2017), were developed to detect the phenols with high sensitivity. These methods always required complex pretreatments, expensive equipment and skilled operators, making it not suitable for rapid analysis. In contrast, colorimetric sensing has drawn special attention because of operational simplicity, easy readout, low cost and high throughput. Notably, some nanozymes as colorimetric receptors have been explored to sensitively monitor the phenols *via* amplifying the signals (Tian et al. 2019; Ma et al. 2020). Yang et al. developed $CeVO_4$ as an oxidase mimic to determine hydroquinone from resorcinol and catechol (Yang et al. 2017). Niu et al. used rGO/Cu_8S_5/PPy as a POD mimic for detection

of phenol (Jiang et al. 2017). Lee's group prepared coral-like silver citrate to be a Laccase mimic to determine different phenols (Koyappayil et al. 2021). By looking through these works, it noticed that the existing nanozyme-based sensors were almost based on the changes of absorption intensity at fixed wavelength, which were easily interfered by sensor concentration, environments and instrumental factors (He et al. 2020). In contrast, ratiometric sensing strategy could resolve these limits *via* providing double or multiple signal outputs. This proposal has been previously reported in fluorescence analysis, in which ratiometric fluorescence emissions were used to quantify the analytes (Zhang et al. 2019). One of the emissions was served as an internal reference to amplify the ratio of signal to noise, realizing sensitive quantification. As far as we known, there were few reports about nanozyme-based colorimetry for ratiometric detection.

The structure of phenols exhibited high degree of heterogeneity, due to different number and position of substituted hydroxyl groups on the benzene ring. This caused their drastically different features in physical and chemical properties, resulting in divergent environment hazard and biological toxicity even at a very low concentration (Czaplicka 2004; Xu et al. 2020). Sensor array was considered to be an extremely practical technology for the discrimination of multiple analogues (Ghasemi et al. 2015). The matrix employed sensing receptor elements to generate distinguishable responses against various targets. With the aid of statistical analysis, these analytes were able to be clustered separately from each other. Compared with "Lock-and-key" recognition mold, there was no necessary to design many specific sensors for each target, drastically cutting down the cost and simplifying assay procedure. In this regard, several colorimetric sensor arrays have been explored to distinguish ions (Najafzadeh et al. 2018), antioxidants (Li et al. 2019) and phenols (Wu et al. 2020) based on their specific influence on catalytic kinetics of nanozymes.

In this study, a POD nanozyme ($Cu_2(OH)_3Cl$) colorimetric senor array has been proposed for ratiometric quantification and discrimination of o-, m- and p-phenols. Copper hydroxychloride ($Cu_2(OH)_3Cl$) showed layered structure composed by edge-sharing HO-Cu-Cl octahedral (Wei et al. 2013; Yang et al. 2016). This tribasic copper salt mainly occurs in three polymorphs, including atacamite (α-$Cu_2(OH)_3Cl$), paratacamite (γ-$Cu_2(OH)_3Cl$) and bollackite (Fleet 1975; Han et al. 2003). Among the polymorphs, γ-$Cu_2(OH)_3Cl$ showed superior affinity to H_2O_2, which was more in favor of enhancement of the POD activity (Wang et al. 2021a). Herein, the single-phase γ-$Cu_2(OH)_3Cl$ were conveniently synthesized to construct a sensor array for diverse phenols.

2. Experimental

2.1 Synthesis of $Cu_2(OH)_3Cl$

$Cu_2(OH)_3Cl$ were prepared as follow: 1.54 g of $CuCl_2{\cdot}2H_2O$ were dissolved in 10 mL ultrapure water (defined as solution A), 2.46 g of 2-methylimidazole were dissolved in 12 mL ultrapure water (solution B), then A and B were fast transferred into 33 mL of isopropanol and stirred for 1 h, the final mixture was

transferred to a 100 mL of Teflon-lined stainless-steel autoclave and kept at 120 ℃ for 8 h. The final product was centrifuged and washed by ethanol for several times, collected samples were dried at 40 ℃ for further applications.

2.2 POD activity of $Cu_2(OH)_3Cl$

Typically, 0.1 mL of H_2O_2 (100 mM), 0.1 mL of TMB (10 mM) and 0.8 mL of $Cu_2(OH)_3Cl$ (0.1 mg/mL) were successfully placed into 1 mL of NaAc-HAc buffer (0.1 M, pH 4.0) with the final volume of 1 mL. Above system was incubated for 30 min at temperature, and the absorbance profile of final products (i.e. TMBox species) were recorded at the wavelength range of 300–700 nm. In order to understand the principle of its POD activity, we have investigated the cyclic voltammetry characteristics for each system (see the detail in ESI). Similarly, ABTS and OPD were also explored for POD activity test, and UV-vis spectra of final products were determined with wavelength from 300 to 700 nm.

2.3 Quantification and discrimination of phenols

In this experiment, four phenolic substances were selected as the target analytes, including p-Dihydroxybenzene (p-DHB), m-Dihydroxybenzene (m-DHB), o-Trihydroxybenzene (o-THB) and phenol. First, 0.8 mL of the $Cu_2(OH)_3Cl$ (0.1 mg/mL) were added into a 4 mL of microcentrifuge tubes. Afterward, a varied concentrations of analytes, 0.1 mL of H_2O_2 (100 mM), 0.1 mL of TMB (10 mM) and 980 μL of NaAc-HAc buffer (0.1 M, pH 4.0) were injected to above systems. After incubation of 30 min at room temperature, the ratio (I_{652}/I_{450}) for each samples were recorded by using UV-vis absorbance spectroscopy.

In order to recognize those phenols separately, a sensor array (6 time points×4 analytes×3 replicates) were designed relying on POD activity of $Cu_2(OH)_3Cl$. All the substances were mixed together following the above procedure. And the concentrations of each analyte were fixed at 0.001 mM, 0.05 mM and 0.5 mM respectively. The raw absorbance data (I_{652}/I_{450}) were subjected to PCA analysis, in which the ellipse areas represent 95% confidence intervals in the PCA pattern.

3. Results And Discussion

3.1 Characterization of $Cu_2(OH)_3Cl$

Figure 1 displayed a X-ray diffraction (XRD) pattern of $Cu_2(OH)_3Cl$, and obvious diffraction peaks were observed at 16.5°, 31.2°, 32.8°, 38.7°, 40°, 50.3° and 53.9°. They were totally indexed to (011), (-121), (013), (202), (023), (033) and (040) lattice planes of paratacamite $Cu_2(OH)_3Cl$ (γ-$Cu_2(OH)_3Cl$, JCPDS 86-1391). Notably, no typical peaks belonging to atacamite $Cu_2(OH)_3Cl$ were observed (α-$Cu_2(OH)_3Cl$, JCPDS 25–0269) (Wang et al. 2021a), indicative of successful single phase fabrication *via* this method. Generally, more alkaline condition was in favor of the recrystallization from α-$Cu_2(OH)_3Cl$ to γ-$Cu_2(OH)_3Cl$ (Pollard et al. 1989). Compared with α-$Cu_2(OH)_3Cl$, the Cu(I) content in γ-$Cu_2(OH)_3Cl$ increased

remarkably and exhibited advanced POD activity *via* Fenton reaction (Wang et al. 2021a). The morphology and microstructure of the $Cu_2(OH)_3Cl$ were further investigated by scanning electron microscopy (SEM) and transmission electron microscopy (TEM). SEM image (Fig. 2a) showed a hierarchical structure of $Cu_2(OH)_3Cl$ sheets with an overall diameter of 20–30 μm. HRTEM image (Fig. 2b) displayed two lattice fringes with spacing of 0.24 nm and 0.22 nm, corresponding to (202) and (023) planes of γ-$Cu_2(OH)_3Cl$. The elemental mappings (Fig. 2c-f) revealed that Cu, O and Cl were homogenously distributed on the surface of γ-$Cu_2(OH)_3Cl$ (Fig,2d) and the atomic ratio of O to Cl reached 2.6∶1. Lower oxygen composition in $Cu_2(OH)_3Cl$ was possible due to existence of oxygen vacancies (O_V), which was generally common in oxides and hydroxides (Ye et al. 2019; Al-Hashem et al. 2019).

XPS analysis were performed to investigate the chemical composition and oxidation states presented in the $Cu_2(OH)_3Cl$. The whole XPS spectrum (Fig. 3a) confirmed the presence of Cu, O and Cl without any impurities. Their atomic percentages obtained were 35.54% (Cu), 45.02% (O) and 19.44% (Cl) respectively. This result was almost consistent with the EDS measurements, further indicative of oxygen deficient in this $Cu_2(OH)_3Cl$. As depicted in Fig. 3b, the binding energies of Cu $2p_{3/2}$ and Cu $2p_{1/2}$ were maxima at 934.7 eV and 954.7 eV respectively. Obviously, Cu^{2+} and Cu^{+} were coexisted in $Cu_2(OH)_3Cl$ since the weak stability in lattices (Lu et al. 2021). Besides, the O 1s XPS spectrum was fitted into three peaks (Fig. 3c), and they were individually assigned to lattice oxygen (O_L)/ hydroxyl (O_{OH}) at 530.7 eV, the oxygen atoms in the vicinity of an oxygen vacancy (O_V) at 531.4 eV and chemisorbed water (O_W) at 532.1 eV (Tang et al. 2020). Being an effective tool for determination of unpaired electrons in materials, Electron paramagnetic resonance (EPR) was further employed to evidence the O_V in $Cu_2(OH)_3Cl$ (Zhang et al. 2016; Hao et al. 2018) (Fig. 3d). The obtained $Cu_2(OH)_3Cl$ represented an obvious EPR signal arising from the electrons trapped on oxygen vacancies. Basically, the peroxidase-like and oxidase-like activities of nanozyme were strongly related with amounts of O_V in the material (Lu et al. 2020; Wang et al. 2022). They were served as active sites for adsorption and activation of O_2 and H_2O_2 (Wang et al. 2021b).

The FTIR spectrum of $Cu_2(OH)_3Cl$ (Fig.S1) displayed three typical peaks at 3309 cm^{-1} 3359 cm^{-1} and 3447 cm^{-1}, corresponding to typical O-H stretches with different atomic distances (d O–H) and hydrogen bond angles (θ O–H···Cl) (Wang et al. 2021a). And the absorption peak located at 1634 cm^{-1} should be attributed to O-H bending vibration. These results demonstrated that the obtained $Cu_2(OH)_3Cl$ was functionalized by amounts of hydroxyl groups. In fingerprint region, besides, the peak was clearly observed at 912 cm^{-1}, attributable to Cu-O-H of copper hydroxychlorides (Zhao et al. 2020). Besides, Fig S2 depicts TG and DTG curves. The decomposition of $Cu_2(OH)_3Cl$ basically displayed two major steps: Initially, 13% mass loss was observed in the range of 187 ℃ to 330 ℃ accompanied with an endothermal peak centered at 263 ℃. This step was caused by dehydration process. The second step was displayed between 330 ℃ and 604 ℃ with an endothermal peak at 542 ℃. It was possibly attributed to the loss of halogen and the formation of CuO, indicative of its strong thermo stability (Bhatta et al. 2021).

3.2 Analysis of POD activity

A typical chromogenic substrate (TMB), was selected to validate the POD activity of $Cu_2(OH)_3Cl$. As shown in Fig. 4a, the TMB, H_2O_2 and $Cu_2(OH)_3Cl$ were mixed together, which represented three absorption peaks located at about 370 nm, 450 nm and 652 nm respectively. Whereas, negligible absorbance was acquired in the absence of the $Cu_2(OH)_3Cl$ or H_2O_2, indicative of superior peroxidase-like property for the $Cu_2(OH)_3Cl$ rather than an oxidase-like activity (Fig. 4a). As illustrated in Fig.S3, there were two kinds of charge-transfer species during the whole peroxidation of TMB, namely single-electron reducing product (TMB-TMB^{++}) and double-electrons reducing product (TMB diamine). The TMB-TMB^{++} represented blue color with the absorbance at 370 nm and 652 nm, and TMB diimine showed yellow color with a peak located at 450 nm (Huang et al. 2018). However, this phenomenon has always been neglected in the previous studies, and investigations were mainly focused on the peak variations at 652 nm (Jiang et al. 2017). As depicted in Fig. 4a, the $Cu_2(OH)_3Cl$-catalyzied product should be a mixture containing above two species. Additionally, some other chromogenic substrates were used to evaluate its catalytic capability, such as 2,2'-azino-bis (3-ethylbenzthiazoline-6-sulfonic acid) (ABTS) and o-phenylenediamine (OPD). Interesting, these two indicators exhibited no responses in the presence of H_2O_2 and $Cu_2(OH)_3Cl$.

In term of catalytic mechanism, the reaction pathways of POD were generally based on the principles of hydroxyl radicals and/or electron transfer (Zheng et al. 2016). To interpret the principle, we first used terephthalic acid (TA) as a fluorescence indicator to study if hydroxyl radicals were produced during the $Cu_2(OH)_3Cl$-catalyzied POD process. Figure 4b showed that there was a weak fluorescence emission at 440 nm (indicative of radical reaction) in the mixture of TA, H_2O_2 and $Cu_2(OH)_3Cl$. However, there were no obvious changes in POD activity when the reaction system was mixed with isopropanol (IPA, a hydroxyl radical quencher) (Fig. 4c). The contradictory results indicated that hydroxyl radicals were indeed generated but they were not the core factor to drive the catalytic process. Besides, Fig. 4d displayed the cyclic voltammograms of $Cu_2(OH)_3Cl$ with and without H_2O_2, of which a remarkable reduction response occurred in the presence of H_2O_2. Obviously, a distinct electron transfer has been triggered during the POD reaction of TMB, which was accelerated by $Cu_2(OH)_3Cl$ as a mediator.

3.3 Ratiometric sensor for determination of phenols

Varied regulations of different phenols on dual-absorbance of TMBox mixture were discovered in Fig. 5. Inspired by the previous works (Wang et al. 2021a), we speculated the interaction between $Cu_2(OH)_3Cl$ and phenols are as follow (Scheme 1): (1) a σ-Cu-ligand complex was formed in which the surface Cu^{2+} of $Cu_2(OH)_3Cl$ combined with the hydroxyls of phenols. (2) Electrons of the phenols were transferred to Cu^{2+} through the complex. (3) In the presence of H_2O_2, the σ-Cu-ligand complex would be cleaved resulting in both the reduction of Cu^{2+} to Cu^{+} and the hydroxylation of aromatic ring, as well as producing hydroxyl radicals during reaction. Integrating with the interaction principles among $Cu_2(OH)_3Cl$, TMBox and phenols, it was reasonable to speculate that electron transfer might be occurred across these three compounds via redox process (Scheme 1).

As depicted in Fig.S4, compared with previous mixture of $Cu_2(OH)_3Cl$, H_2O_2 and TMB, a new oxidation peak was obviously seen in the cyclic voltammograms after addition of o-THB. Further, the oxidation peak for o-THB was significantly stronger than that of m-DHB (Fig.S5). It's indicated that electron transfer was triggered among $Cu_2(OH)_3Cl$, phenols and TMBox species. In addition, because of varied steric hindrances and reducing ability, different electron transfer pathways occurred for each phenol, resulting in distinguished composition of TMBox species and colorimetric signal outputs. The difference of electrochemical features between o-THB and m-DHB confirmed this speculation. With this consideration, the POD-like $Cu_2(OH)_3Cl$ could be employed as a receptor element in the colorimetric sensor array for discrimination of various phenols.

Figure 5a-5d showed the absorption titration measurements to investigate feasibility of $Cu_2(OH)_3Cl$-based sensing system for m-DHB, p-DHB, o-THB and phenol. Upon gradual addition of each target, the absorption peaks at 450 nm and 652 nm displayed different changes in intensity. In the presence of m-DHB, for example, the typical peak of TMB-TMB^{++} at 652 nm deceased sharply, and that of TMB diimine at 450 nm remained unchanged (Fig. 5a). Figure 6a showed that the I_{652}/I_{450} deceased linearly with the increased levels of m-DHB ranging from 20 to 1000 μM (I_{652}/I_{450} = 6.303-0.0036C, R^2 = 0.98). Interestingly, the I_{652}/I_{450} feature for o-THB showed resemblance with that of m-DHB (Fig. 5b), but the linear range was from 0 to20 μM (Fig. 6b). As for p-DHB, both absorption peak at 652 nm and 450 nm were decreased linearly in the level of 0–20 μM (Fig. 5c and Fig. 6c). As shown in Fig. 5d, the sensing system was obvious insensitive to phenol where both of absorbance were almost unchanged. Consequently, the LODs of m-DHB, p-DHB and o-THB were 12.25, 0.0124 and 0.004 μM, respectively. The favorable performance should be arising from the dual-signal outputs of our colorimetric assay. Although the LOD was still inferior to that of mass spectrometry and Western blot, and the current analytical system would be improved if increasing POD activity of $Cu_2(OH)_3Cl$.

3.4 Colorimetric sensor array for discrimination of phenols

Since different impacts of each phenols on I_{652}/I_{450}, it was available to design an effective colorimetric sensor array based on $Cu_2(OH)_3Cl$ to discriminate them. In this regard, four phenols (i.e., m-DHB, p-DHB, o-THB and phenol) were selected as the analytes to testify feasibility of this sensor array. Fig.S6 showed varied time-dependent plots of I_{652}/I_{450} among these phenols, providing a necessity to realize their discrimination. According to data of Fig.S6, the fingerprints have been extracted from the absorbance ratio (I_{652}/I_{450}) at a series of time points ranging from 10 to 60 min (Fig. 7a). After three parallel measurements, a two-dimensional PCA pattern was studied according to the data from fingerprints (6 time points × 4 analytes×3 replicates). As shown in Fig. 7b, four isolated groups were distinctly classified with no overlaps. In addition, similar PCA patterns were explored in varied concentrations of phenols. As shown in Fig. 7c and 7d, well-defined classifications were also observed in each pattern. These indicated that the sensor array displayed excellent reliability in a broad of concentration level. To explore the robustness of sensing strategy, we randomly tested 6 unknown samples (Table S1). The whole

measurements were performed by comparing with the PCA pattern in Fig. 7. Obviously, all the unknown samples have been identified correctly, further confirming its availability in real applications.

4. Conclusion

In summary, we have developed a ratiometric colorimetric sensor array for determination of varied phenols. This sensor array was carried out via $Cu_2(OH)_3Cl$-mediated regulation of TMBox species by phenols. Diverse phenols triggered different changes in absorbance at 652 nm and 450 nm, resulting in variations in I_{652}/I_{450} and color of solution. Through linear relationship between I_{652}/I_{450} and concentration of each phenol, quantification of targets has successfully performed. In addition, PCA plots obtained from fingerprints were carried out for discrimination of o-, m- and p-phenols even at a level of 0.001 mM. Moreover, this strategy exhibited excellent robustness in recognition of blind samples. In contrast with previous assays, this ratiometric sensor array showed higher accuracy and selectivity to phenols, and there is no needed to prepare substantial specific recognition receptors for targets.

Declarations

Authors' Contributions

Lan C. performed the experiments, analyzed the results, and wrote the manuscript; Meng L. edited the manuscript; Xu N. reviewed the manuscript.

Funding Information

This study was financially supported by Jilin Scientific and Technological Development Program (CN) (No. YDZJ202101ZYTS174), and the authors acknowledge the assistance of JLICT Center of Characterization and Analysis.

Compliance with Ethical Standards

Conflict of Interest

The authors declare no competing interests.

Availability of data and materials

Data sharing not applicable to this article as no datasets were generated or analyzed during the current study.

Ethical Approval

This article does not contain any studies with human participants or animals performed by any of the authors.

Informed Consent

Informed consent is not applicable in this study.

References

1. Al-Hashem M, Akbar S, Morris P (2019) Role of oxygen vacancies in nanostructured metal-oxide gas sensors: a review. Sensor Actuat B-Chem 301: 126845.
2. Arfin T, Sonawane K, Tarannum A (2019) Review on detection of phenol in water. Adv Mater Lett 10: 753-785
3. Bhatta LKG, Gundanna SK, Venkatesh K, Bhatta UM (2021) Microwave-assisted novel one-pot synthesis and characterization of copper oxide. Chem Paper 75: 2597-2601
4. Cheng TS, Nasir MZM, Ambrosi A, Pumera M (2017) 3D-printed metal electrodes for electrochemical detection of phenols, Appl Mater Today 9: 212-219
5. Chernonosov AA, Karpova EA, Lyakh EM (2017) Identification of phenolic compounds in Myricaria bracteata leaves by high-performance liquid chromatography with a diode array detector and liquid chromatography with tandem mass spectrometry. Rev Bras Farmacogn 27: 576-579
6. Czaplicka M (2004) Sources and transformations of chlorophenols in the natural environment. Sci Total Envir 322: 21-39
7. Du L, Ma L, Qiao Y, Lu Y, Xiao D (2016) Determination of phthalate esters in teas and tea infusions by gas chromatography-mass spectrometry. Food Chem 197: 1200-1206
8. Fleet M (1975) The crystal structure of paratacamite, $Cu_2(OH)_3Cl$. Acta Crystallogr B 31: 183-187
9. Ghasemi F, Hormozi-Nezhad MR, Mahmoudi M (2015) A colorimetric sensor array for detection and discrimination of biothiols based on aggregation of gold nanoparticles. Anal Chim Act 882: 58-67
10. Han MS, Lee BG, Ahn BS, Kim HS, Moon DJ, Hong SI (2003) The role of copper chloride hydroxides in the oxidative carbonylation of methanol for dimethyl carbonate synthesis. J Molecul Catal A Chem 203: 137-143
11. Hao J, Peng S, Li H, Dang S, Qin T, Wen Y, Huang J, Ma F, Gao D, Li F (2018) A low crystallinity oxygen-vacancy-rich Co_3O_4 cathode for high-performance flexible asymmetric supercapacitors. J Mater Chem A 6: 16094-16100
12. He S-B, Balasubramanian P, Hu A-L, Zheng X-Q, Lin M-T, Xiao M-X, Peng H-P, Deng H-H, Chen W (2020) One-pot cascade catalysis at neutral pH driven by CuO tandem nanozyme for ascorbic acid and alkaline phosphatase detection. Sensor Actuat B-Chem 321 128511
13. Huang W, Xie Z, Deng Y, He Y (2018) 3, 3', 5, 5'-tetramethylbenzidine-based quadruple-channel visual colorimetric sensor array for highly sensitive discrimination of serum antioxidants. Sensor Actuat B-Chem 254, 1057-1060.
14. Jiang Y, Gu Y, Nie G, Chi M, Yang Z, Wang C, Wei Y, Lu X (2017) Synthesis of RGO/Cu_8S_5/PPy Composite Nanosheets with Enhanced Peroxidase-Like Activity for Sensitive Colorimetric Detection

of H_2O_2 and Phenol. Part Part Syst Char 34: 1600233

15. Karim F, Fakhruddin A N M (2012) Recent advances in the development of biosensor for phenol: a review. Rev Environ Sci Bio 11(3): 261-274.
16. Koyappayil A, Kim HT, Lee M-H (2021) 'Laccase-like'properties of coral-like silver citrate micro-structures for the degradation and determination of phenolic pollutants and adrenaline. J Hazar Mater 412: 125211
17. Li X, Kong C, Chen Z (2019) Colorimetric sensor arrays for antioxidant discrimination based on the inhibition of the oxidation reaction between 3, 3', 5, 5'-tetramethylbenzidine and hydrogen peroxides. Acs Appl Mater Inter 11: 9504-9509
18. Lu J, Zhang H, Li S, Guo S, Shen L, Zhou T, Zhong H, Wu L, Meng Q, Zhang Y (2020) Oxygen-vacancy-enhanced peroxidase-like activity of reduced Co_3O_4 nanocomposites for the colorimetric detection of H_2O_2 and glucose. Inorg Chem 59(5): 3152-3159.
19. Lu Q, Jiang H, Cheng R, Xia S, Zhan K, Yi T, Morrell JJ, Yang L, Du G, Gao W (2021) Preparation of superhydrophobic wood surfaces via in-situ synthesis of $Cu_2(OH)_3Cl$ nano-flowers and impregnating PF&STA to improve chemical and mechanical durability. Ind Crop Prod 172, 113952.
20. Ma X, He S, Zhang Y, Xu J, Zhang H, Wang Z, Xue J, Li X, Yu W, Fan X (2020) Signal-off tuned signal-on (SF-T-SN) colorimetric immunoassay for amantadine using activity-metalmodulated peroxidase-mimicking nanozyme. Sensor Actuat B-Chem 311: 127933
21. Michałowicz J, Duda W (2007) Phenols–Sources and Toxicity. Polish Journal of Environmental Studies 16(3)
22. Najafzadeh F, Ghasemi F, Hormozi-Nezhad MR (2018) Anti-aggregation of gold nanoparticles for metal ion discrimination: a promising strategy to design colorimetric sensor arrays. Sensor Actuat B-Chem 270: 545-551
23. Pollard A M, Thomas R G, Williams P A (1989) Synthesis and stabilities of the basic copper (II) chlorides atacamite, paratacamite and botallackite. Mineral Mag 53: 557-563
24. Qi J, Li B, Wang X, Fu L, Luo L, Chen L (2018) Rotational paper-based microfluidic-chip device for multiplexed and simultaneous fluorescence detection of phenolic pollutants based on a molecular-imprinting technique, Analy Chem 90: 11827-11834
25. Tang Y, Shen H, Cheng J, Liang Z, Qu C, Tabassum H, Zou R (2020) Fabrication of oxygen-vacancy abundant NiMn-layered double hydroxides for ultrahigh capacity supercapacitors. Advanced Functional Materials 30(11): 1908223.
26. Tian F, Zhou J, Jiao B, He Y (2019) A nanozyme-based cascade colorimetric aptasensor for amplified detection of ochratoxin A. Nanoscale 11(19): 9547-9555
27. Wang H, Zhang Z, Yin H, Wu Y (2021a) Synthesis of $Cu_2(OH)_3Cl$ as facile and effective Fenton catalysts for mineralizing aromatic contaminants: Combination of σ-Cu-ligand and self-redox property. Appl Catal A Gen 614: 118055

28. Wang X, Wen F, He L, Su J, Jiang P, He D (2022) Engineering porous Co–Mn oxide nanosheets with abundant oxygen vacancy as an efficient oxidase-like mimic for heparin colorimetric sensing. Anal Chim Acta 1198: 339564.
29. Wang Z, Shen X, Gao X (2021b). Density Functional Theory Mechanistic Insight into the Peroxidase- and Oxidase-like Activities of Nanoceria. J Phys Chem C 125(42): 23098-23104.
30. Wei W, Gao P, Xie J, Zong S, Cui H, Yue X (2013) Uniform $Cu_2Cl(OH)_3$ hierarchical microspheres: a novel adsorbent for methylene blue adsorptive removal from aqueous solution. J Solid State Chem 204: 305-313
31. Wu S, Guo D, Xu X, Pan J, Niu X (2020) Colorimetric quantification and discrimination of phenolic pollutants based on peroxidase-like Fe_3O_4 nanoparticles. Sensor Actuat B-Chem 303: 127225
32. Xu X, Wu S, Guo D, Niu X (2020) Construction of a recyclable oxidase-mimicking Fe_3O_4@MnO_x-based colorimetric sensor array for quantifying and identifying chlorophenols. Anal Chim Act 1107: 203-212
33. Yang H, Barton IF, Andrade MB, Downs RT (2016) Crystal structure of a new compound, $CuZnCl(OH)_3$, isostructural with botallackite. Am Mineral 101: 986-990
34. Yang H, Zha J, Zhang P, Qin Y, Chen T, Ye F (2017) Fabrication of $CeVO_4$ as nanozyme for facile colorimetric discrimination of hydroquinone from resorcinol and catechol. Sensor Actuat B-Chem 247: 469-478
35. Ye K, Li K, Lu Y, Guo Z, Ni N, Liu H, Huang Y, Ji H, Wang P (2019) An overview of advanced methods for the characterization of oxygen vacancies in materials. TrAC-Trend Anal Chem 116: 102-108.
36. Zhang N, Li X, Ye H, Chen S, Ju H, Liu D, Lin Y, Ye W, Wang C, Xu Q (2016) Oxide defect engineering enables to couple solar energy into oxygen activation. J Am Chem Soc 138: 8928-8935
37. Zhang P, Li S, Fu C, Zhang Q, Xiao Y, Ding C (2019) A colorimetric and near-infrared ratiometric fluorescent probe for the determination of endogenous tyrosinase activity based on cyanine aggregation. Analyst 144: 5472-5478
38. Zhao Y, Cui H, Zhang J, Ma Y, Tian H, Wu L, Cui Q, Ma Y (2020) Pressure-Induced Phase Transformation of Botallackite α-$Cu_2(OH)_3Cl$ with a Two-Dimensional Layered Structure Synthesized *via* a Hydrothermal Strategy. J Phys Chem C 124: 9581-9590
39. Zheng C, Ke W, Yin T, An X (2016) Intrinsic peroxidase-like activity and the catalytic mechanism of gold@ carbon dots nanocomposites. RSC Adv 6: 35280-35286

Scheme

Scheme 1 is available in the Supplementary Files section

Figures

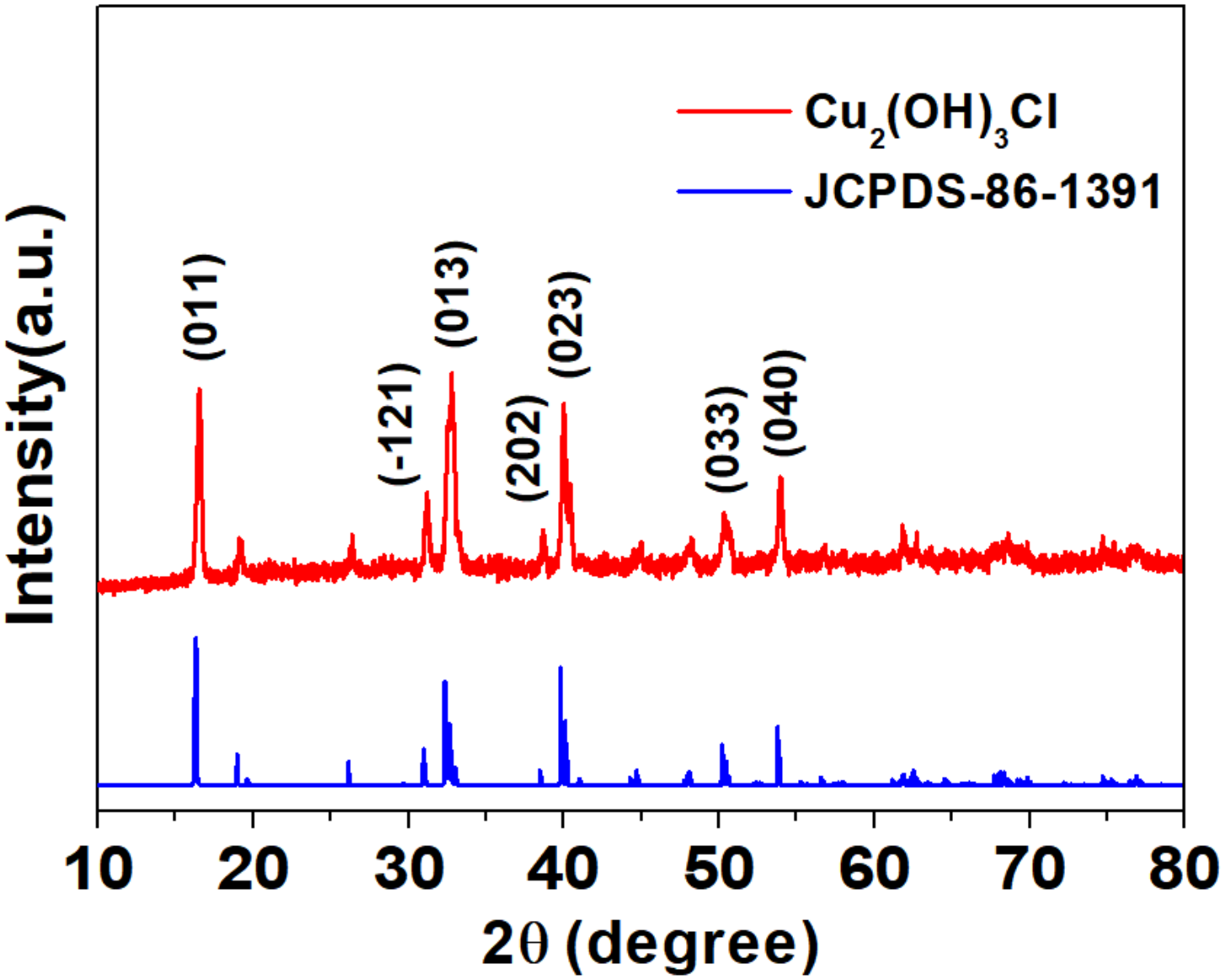

Figure 1

XRD pattern of obtained $Cu_2(OH)_3Cl$.

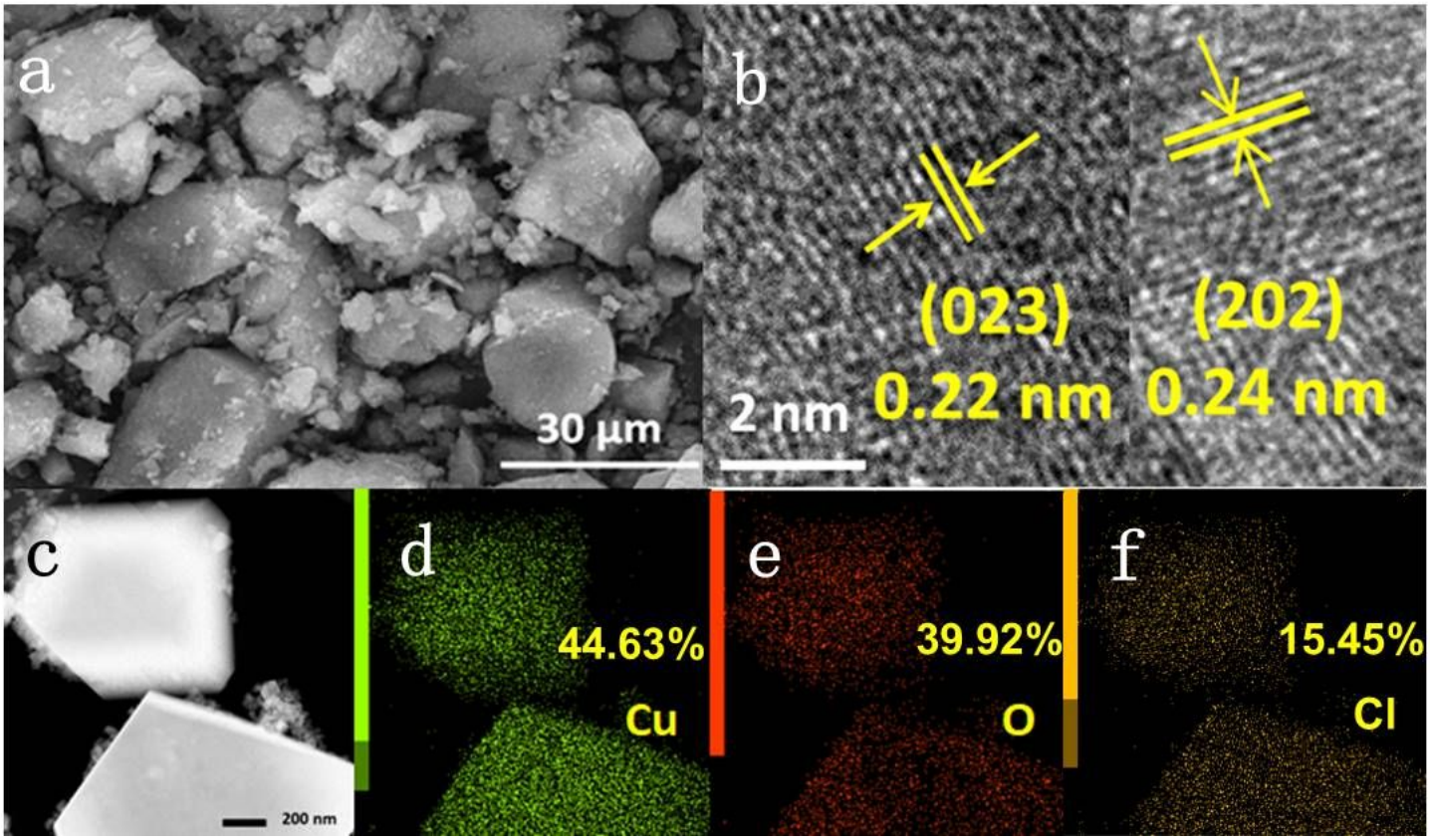

Figure 2

(a) SEM (scale bar 30 mm) and (b) HRTEM images (scale bar 2 nm) of $Cu_2(OH)_3Cl$. (c) High-angle annular dark-field scanning transmission electron microscopy (HAADF-STEM) and (d-f) corresponding EDS mapping of $Cu_2(OH)_3Cl$ (scale bar 200 nm).

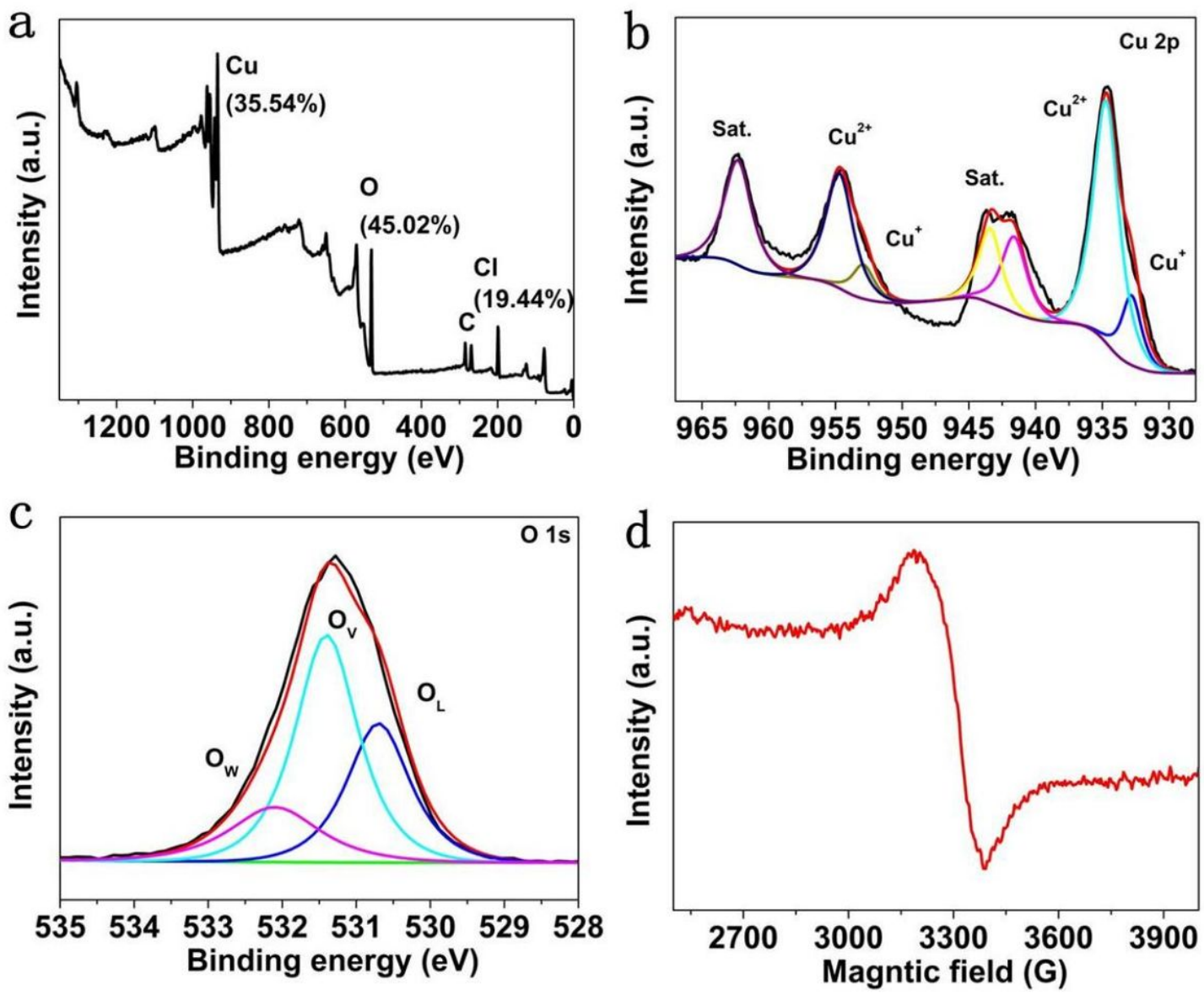

Figure 3

XPS results of $Cu_2(OH)_3Cl$: (a) full spectrum, (b) Cu 2p, (c) O 1s. (d) The corresponding ESR spectrum.

Figure 4

(a) UV-vis absorbance profiles of reaction systems in the presence of $Cu_2(OH)_3Cl$ and TMB (black line), H_2O_2 and TMB (red line), $Cu_2(OH)_3Cl$ and H_2O_2 (blue line), as well as mixture of above three species (pink line). (b) Fluorescence spectra of $Cu_2(OH)_3Cl$+H_2O_2 mixture before and after addition of TA. (c) Catalytic kinetics analysis of reaction system with and without IPA. (d) Cyclic voltammograms of obtained $Cu_2(OH)_3Cl$ before and after addition of H_2O_2.

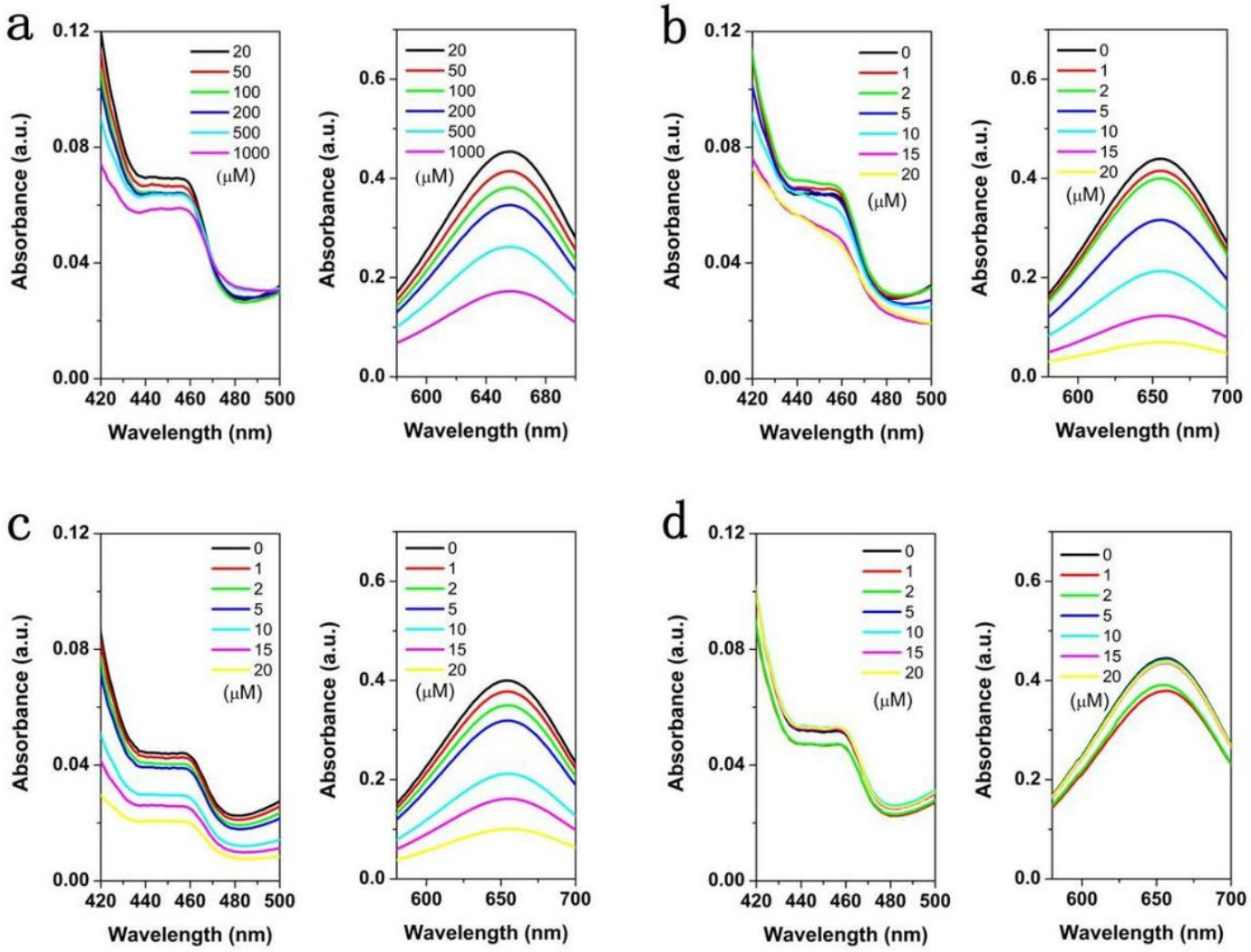

Figure 5

UV–vis absorbance results of the reaction system ($Cu_2(OH)_3Cl$, H_2O_2 and TMB) in the presence of different concentrations of (a) m-DHB, (b) o-THB, (c) p-DHB and (d) phenol.

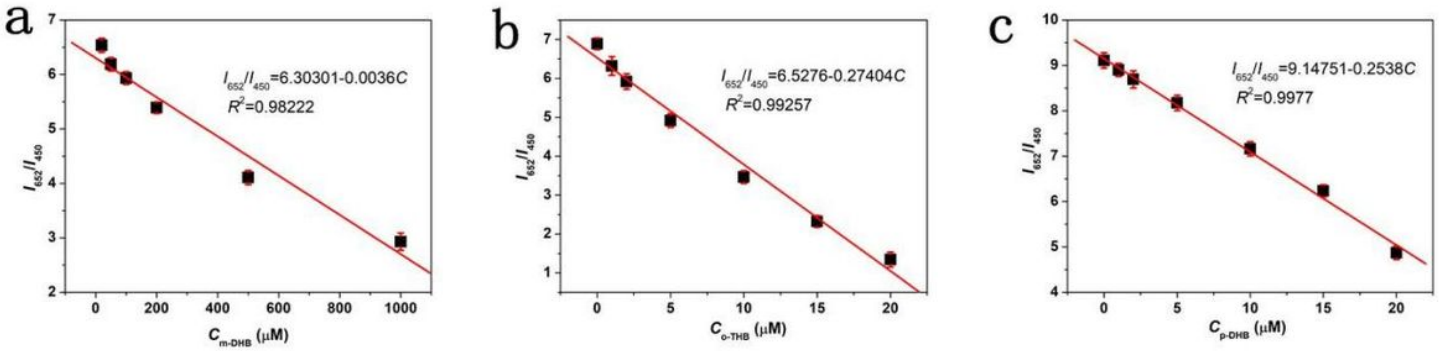

Figure 6

The relationship between I_{652}/I_{450} and concentration of corresponding phenols: (a) m-DHB, (b) o-THB, (c) p-DHB, and the error bars represent the standard deviation of three repetitive measurements.

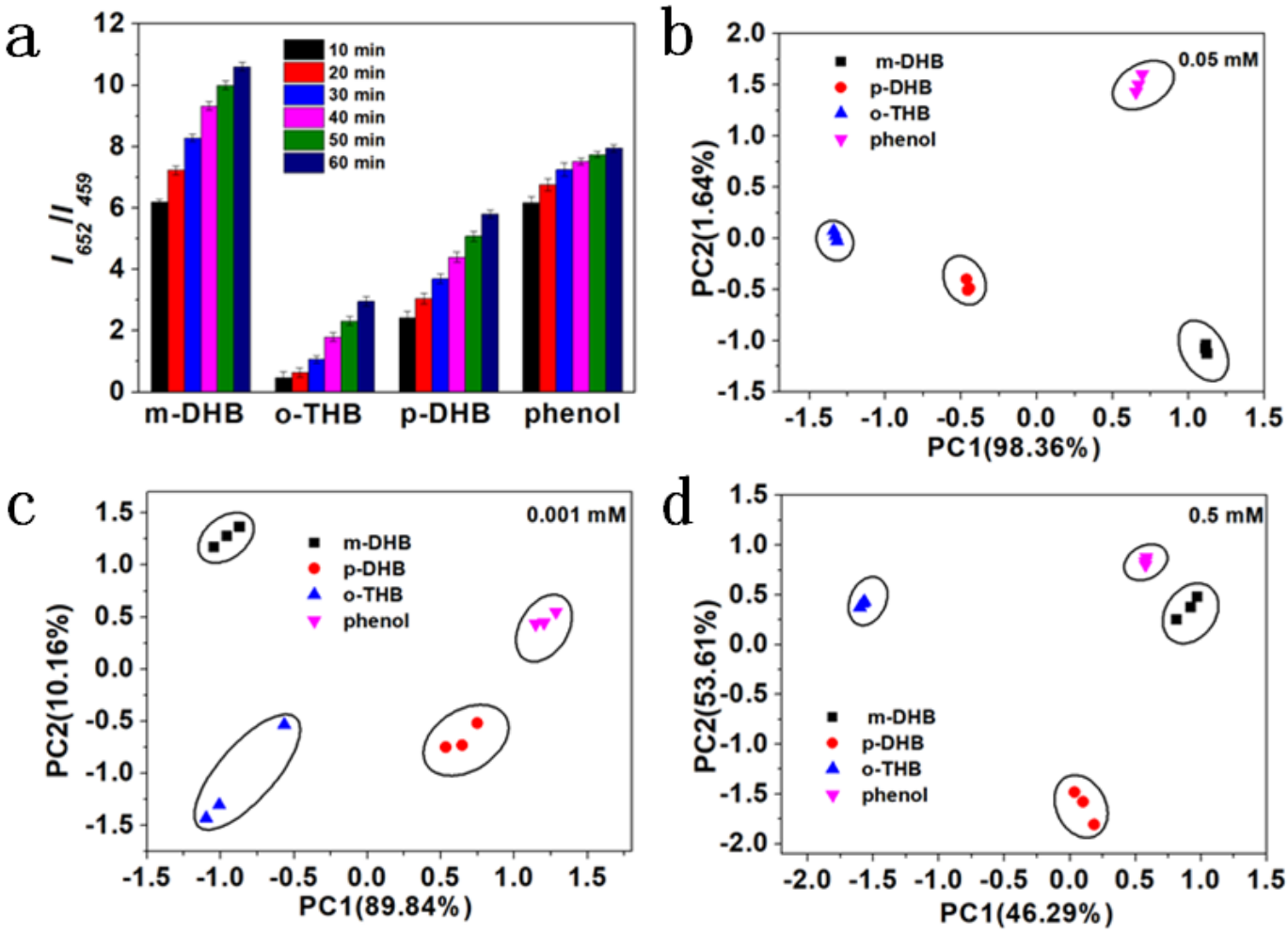

Figure 7

(a) The fingerprint profiles of four kinds of phenols. (b-d) The PCA patterns for discriminating phenols with 0.001, 0.05 and 0.5 mM.

Supplementary Files

This is a list of supplementary files associated with this preprint. Click to download.

- ESI20220503.docx
- floatimage6.jpeg